Quantum entanglement in plasmonic waveguides with near-zero mode indices

Xing Ri Jin, Lei Sun, Xiaodong Yang, and Jie Gao*

Department of Mechanical and Aerospace Engineering, Missouri University of Science and Technology, Rolla, Missouri 65409, USA
**Corresponding author: gaojie@mst.edu*

Received July 29, 2013; revised September 16, 2013; accepted September 17, 2013;
posted September 19, 2013 (Doc. ID 194543); published October 9, 2013

We investigate the quantum entanglement between two quantum dots (QDs) in a plasmonic waveguide with a near-zero mode index, considering the dependence of concurrence on interdot distance, QD waveguide frequency detuning, and coupling strength ratio. High concurrence is achieved for a wide range of interdot distances due to the near-zero mode index, which largely relaxes the strict requirement of interdot distance in conventional dielectric waveguides or metal nanowires. The proposed QD waveguide system with near-zero phase variation along the waveguide near the mode cutoff frequency shows very promising potential in quantum optics and quantum information processing.

OCIS codes: (250.5403) Plasmonics; (270.0270) Quantum optics; (270.5580) Quantum electrodynamics.
http://dx.doi.org/10.1364/OL.38.004078

Highly entangled quantum states play important roles in quantum information science, such as schemes for quantum cryptography, quantum teleportation, and quantum computation [1–4]. Among different physical realizations, scalable solid-state quantum entanglement is the most promising one, and the recent successes of quantum entanglement have been obtained with quantum dots (QDs) or diamond nitrogen vacancy centers [5–8] in the visible frequency range. For long-distance entanglement, the correlation between two spatially separated qubits is usually mediated by photons. However, instead of the photon, the surface plasmon [9] has attracted much attention, since it reveals a strong analogy to light propagation in conventional dielectric optical components. Plasmonic waveguides and resonators can be used to confine light to subwavelength dimensions below the diffraction limit to achieve photonic circuit miniaturization [10], and furthermore, they strongly interact with quantum emitters for the applications of detectors, transistors, and quantum information processing [11–14]. For a one-dimensional plasmonic waveguide, the scattering properties of surface plasmons interacting with QDs have been studied widely [15–20]. Recently, Chen *et al.* [21] and Gonzalez-Tudela *et al.* [22] have reported quantum entanglement generation between two separated QDs mediated by a plasmonic waveguide. A highly entangled state between QDs can be achieved only when the interdot distance is controlled with specific values, due to the sinusoidal phase variation of the propagating surface plasmon mode in the waveguide.

In this work, we examine plasmonic waveguides with near-zero mode indices and investigate the quantum entanglement between two QDs simultaneously interacting with the waveguide mode. High concurrence of the entangled state can be obtained for a wide range of interdot distances d and QD–waveguide coupling strength ratios g_2/g_1, showing the great advantage of relaxing the strict requirements of QD positions in comparison to previous schemes. The physical mechanism of the interdot distance flexibility is the vanishing phase variation between two arbitrary positions along a plasmonic waveguide with a near-zero mode index. With the pioneering experimental verification of $n = 0$ structures for visible light by Vesseur *et al.* [23], the proposed QD–waveguide platform is certain to be a promising experimental platform for realizing highly entangled quantum states.

Figure 1(a) shows a schematic of one SiO_2/Ag waveguide engineered to exhibit a near-zero mode index in the visible frequency range. The diameter of the SiO_2 core is D, which is fully surrounded by a thick silver cladding. The permittivity of silver is described by the Drude model, with a plasmon frequency ω_p of 1.37×10^{16} rad/s and a collision frequency γ of 8.5×10^{13} rad/s at room temperature. The refractive index of SiO_2 is 1.46. A pair of QDs, each of which has one excited state $|e\rangle$ and one ground state $|g\rangle$, are embedded in the SiO_2/Ag waveguide as illustrated in Fig. 1(b). $\delta(\Delta) = \omega_k - \omega_{1(2)}$ is the frequency detuning between the incident waveguide mode and the QD exciton transition. d is the interdot distance between the two separated QDs.

The mode indices n of SiO_2/Ag plasmonic waveguides are plotted in Fig. 2(a), where the loss of Ag is neglected. A near-zero mode index can be reached around the cutoff frequency of the waveguide mode, which can be designed by varying the waveguide diameter. The working wavelength with a near-zero mode index can be controlled from the visible 685 nm to the near-IR 920 nm when the waveguide diameter D changes from 100 to 150 nm. Regarding the experimental condition at a cryogenic temperature for the interaction between visible QDs and the waveguide mode, a silver cladding layer with a 0.1γ damping rate

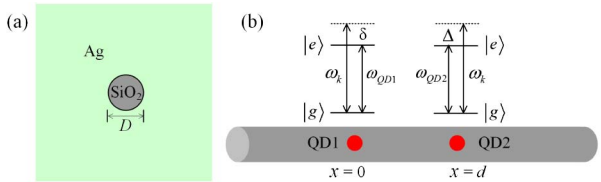

Fig. 1. (a) Schematic of the cross section of a SiO_2 waveguide with a thick silver cladding. D is the diameter of the SiO_2 core. A 3 μm long waveguide is used in the model. (b) Pair of two-level QDs separated by distance d interacting with the waveguide mode. $\delta(\Delta)$ is the frequency detuning between the QD_1 (QD_2) transition and the incident waveguide mode.

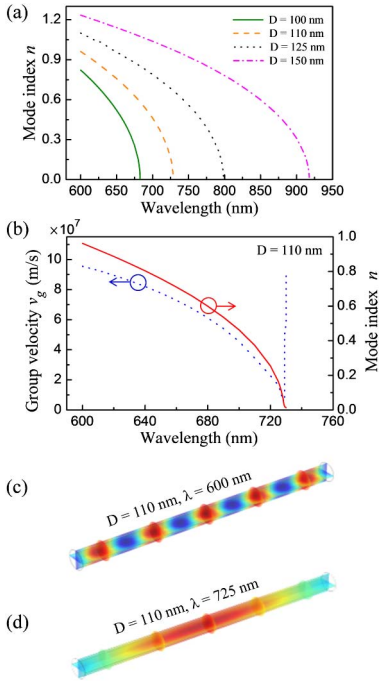

Fig. 2. (a) Dependence of waveguide mode indices n on the wavelengths for different diameters D at 100 nm (greensolid line), 110 nm (orange-dashed line), 125 nm (navy-dotted line), and 150 nm (magenta dashed–dotted line); (b) dependence of group velocity v_g and mode index n on the wavelengths for the waveguide with $D = 110$ nm when 0.1γ Ag loss is considered; (c) and (d) the electric field distributions at the wavelengths of 600 and 725 nm for the waveguide in (b).

and waveguide of $D = 110$ nm is considered in the following analysis. Figure 2(b) shows the corresponding mode index n and group velocity v_g, where the mode index gradually approaches a vanishing small number and the group velocity slows down to $c/42$ at a wavelength of 728.6 nm. Group velocity v_g is calculated according to $v_g = c/(n + \omega(dn/d\omega))$, where c is the speed of light in vacuum. Figures 2(c) and 2(d) show electric field distributions at wavelengths of 600 and 725 nm for the SiO_2/Ag waveguide calculated in Fig. 2(b). The corresponding mode indices at the wavelengths of 600 and 725 nm are 0.962 and 0.164, respectively. For the waveguide mode with a near-zero index, light can propagate along the waveguide with a spatially uniform phase, near-infinity phase velocity, and slow group velocity.

Here, we consider the incident waveguide mode with energy $E_k = v_g k$ interacting simultaneously with two QDs, where k is the wave vector of the incident mode. Thus the real-space Hamiltonian can be written as (assuming $\hbar = 1$)

$$H = \int \mathrm{d}x \Big\{ -iv_g c_R^\dagger(x)\frac{\partial}{\partial x}c_R(x) + iv_g c_L^\dagger(x)\frac{\partial}{\partial x}c_L(x) + \sum_{j=1}^{2} g_j \delta[x-(j-1)d][c_R^\dagger(x)\sigma_-^j + c_R(x)\sigma_+^j + c_L^\dagger(x)\sigma_-^j + c_L(x)\sigma_+^j] \Big\} + \sum_{j=1}^{2}\left(\omega_j - i\frac{\Gamma}{2}\right)\sigma_{e_j,e_j}, \quad (1)$$

where $c_R^\dagger(x)$ $[c_L^\dagger(x)]$ is the bosonic operator creating a right-going (left-going) surface plasmon at the position x, and $g_j (j = 1, 2)$ is the coupling strength between individual QDs and the waveguide mode. Here, the dipole moments of the two QDs have the same orientation and both dipole moments are parallel to the polarization direction of the waveguide mode. $\sigma_{e_j,e_j} = |e\rangle_j\langle e|$ represents the diagonal element of the j th QD operator, and $\sigma_+^j = |e\rangle_j\langle g|(\sigma_-^j = |g\rangle_j\langle e|)$ represents the rasing (lowering) operator. ω_j is the transition frequency of the jth QD, and Γ is the total dissipation including the exciton decay to free space, ohmic loss, and other dissipative channels. The eigenstate of the system can be written as

$$\begin{aligned}|E_k\rangle = \int \mathrm{d}x [&\phi_{k,R}^+(x)c_R^\dagger(x) + \phi_{k,L}^+(x)c_L^\dagger(x)]|g_1,g_2\rangle|0\rangle_{\mathrm{sp}} \\ &+ \xi_{k_1}|e_1,g_2\rangle|0\rangle_{\mathrm{sp}} + \xi_{k_2}|g_1,e_2\rangle|0\rangle_{\mathrm{sp}}, \end{aligned} \quad (2)$$

where ξ_{k_1} (ξ_{k_2}) is the probability amplitude that QD_1 (QD_2) absorbs the waveguide mode and jumps to its excited state. Supposing a surface plasmon incident from the left, the scattering amplitudes can be written as $\phi_{k,R}^+(x) \equiv e^{ikx}[\theta(-x) + a\theta(x)\theta(d-x) + t\theta(x-d)]$ and $\phi_{k,L}^+(x) \equiv e^{-ikx}[r\theta(-x) + b\theta(x)\theta(d-x)]$. $\theta(x)$ is the unit step function, which equals unity when $x \geq 0$ and zero when $x < 0$. a and b are the probability amplitudes of the field between the two QDs at $x = 0$ and $x = d$. t and r are the transmission and reflection amplitudes, respectively. By solving the eigenvalue equation $H|E_k\rangle = E_k|E_k\rangle$, one can obtain the following relations for the coefficients:

$$\begin{aligned} &g_1(1 + a + r + b) = \left(\delta + \frac{i\Gamma}{2}\right)\xi_{k_1}, \\ &g_2(2ae^{ikd} + 2be^{-ikd}) = \left(\Delta + \frac{i\Gamma}{2}\right)\xi_{k_2}, \\ &a = 1 + \frac{g_1\xi_{k_1}}{iv_g}, \qquad t = 1 + \frac{1}{iv_g}(g_1\xi_{k_1} + g_2\xi_{k_2}e^{-ikd}), \\ &b = \frac{g_2\xi_{k_2}}{iv_g}e^{ikd}, \qquad r = \frac{1}{iv_g}(g_1\xi_{k_1} + g_2\xi_{k_2}e^{ikd}). \end{aligned} \quad (3)$$

Through solving the Eq. (3), ξ_{k_1} and ξ_{k_2} can be obtained as follows:

$$\begin{aligned} \xi_{k_1} &= \frac{-i4g_1[-4(-1+e^{2ikd})J_2 + (\Gamma - 2i\delta)]}{\eta}, \\ \xi_{k_2} &= \frac{-i4g_2e^{ikd}(\Gamma - 2i\Delta)}{\eta}, \\ \eta &= -16(-1+e^{2ikd})J_1^2J_2^2 + 4[J_1(\Gamma - 2i\delta) \\ &\quad + J_2(\Gamma - 2i\Delta)] + (\Gamma - 2i\delta)(\Gamma - 2i\Delta), \end{aligned} \quad (4)$$

where $J_1 = g_1^2/v_g$ and $J_2 = g_2^2/v_g$. If there is no transmission and reflection observed by detectors at the two ends of the waveguide, the state of the system is projected to $\xi_{k_1}|e_1,g_2\rangle|0\rangle_{\mathrm{sp}} + \xi_{k_2}|g_1,e_2\rangle|0\rangle_{\mathrm{sp}}$, which means that the

entangled state between the two QDs has been generated. The degree of entanglement can be measured [24,25] by the concurrence $C = \max(\lambda_1 - \lambda_2 - \lambda_3 - \lambda_4, 0)$. $\lambda_i (i = 1, 2, 3, 4)$ are the square roots of the eigenvalues of the matrix $R = \rho(\sigma_y \otimes \sigma_y)\rho^*(\sigma_y \otimes \sigma_y)$, where ρ is the density matrix of the system and σ_y is the Pauli matrix. For the system of two QDs, concurrence C takes the form of $C = ((2|\xi_{k_1}||\xi_{k_2}|)/(|\xi_{k_1}|^2 + |\xi_{k_2}|^2))$. Maximum entanglement can be created when amplitude $|\xi_{k_1}|$ is equal to $|\xi_{k_2}|$.

First, we examine the dependence of the concurrence on waveguide mode index, interdot distance, and QD–waveguide coupling strengths in the model. Figure 3 shows the concurrence C as a function of the interdot distance d and the plasmonic waveguide mode index n when the coupling strength $g_1 = g_2$. We take the same detuning $\Delta = \delta$ between two QDs and the waveguide mode (thus $J = J_1 = J_2$) for simplicity in the following discussion. Clearly, in Fig. 3(b), when the incident waveguide mode is off-resonance with QDs ($\Delta = 0.5J$), the concurrence C is higher than in the on-resonant case shown in Fig. 3(a) over a wide range of mode indices and interdot distances. For conventional waveguide modes with nonzero mode indices, maximum entanglement can be achieved if the two QDs are placed at the right locations, where the interdot distance d is equal to a multiple half-wavelength of the waveguide mode. However, when the plasmonic waveguide mode index n gets close to zero, the concurrence remains above 0.9 over a wide range of interdot distances. The relaxed distance requirement strongly overcomes the challenges of precise QD position control in practical situations.

When the coupling strengths between QDs and the waveguide mode are not identical, the dependence of the concurrence C as a function of the ratio g_2/g_1 is plotted in Fig. 4 when $\Delta = 0.5J_1$. In Fig. 4(a), when the mode index $n = 0$, maximum concurrence C around unity can be created for any arbitrary interdot distance when $g_2 = g_1$, and the concurrence decreases when the difference between g_2 and g_1 increases. This phenomenon shows that the amplitudes ξ_{k_1} and ξ_{k_2} always have the same value in the case of $g_1 = g_2$ and $n = 0$, which results in the concurrence $C = 1$. Even when the mode index cannot reach exact zero in practical situations, for example, $n = 0.1$, high concurrence C can still be achieved within a relatively broad range of interdot distances d and g_2/g_1 ratios. The dark red region in Fig. 4(b) highlights that a high concurrence can be obtained as long as $d < 100$ nm and $1 < g_2/g_1 < 4$, which significantly relaxes the strict conditions required in conventional waveguides.

Next, we discuss concurrence of the entanglement state between two QDs in a practical $D = 110$ nm SiO_2/Ag waveguide with dispersion, as illustrated in Fig. 2(b). Figure 5(a) shows the concurrence C when the waveguide mode index $n = 0.022$, 0.164, 0.462, and 0.962. A near-zero mode index can be chosen by working near the cutoff wavelength of the waveguide mode. The corresponding group velocities v_g are 0.82×10^7 m/s, 1.65×10^7 m/s, 3.44×10^7 m/s, and 9.55×10^7 m/s, respectively. For other parameters of the QD waveguide device, coupling strength $g_1 = g_2 = 35$ GHz, detuning $\Delta = 0.5J$ with $J = J_1 = J_2$, and total dissipation $\Gamma = 500$ GHz. When n is 0.962, the maximum value of concurrence occurs at two locations [green dashed–dotted line in Fig. 5(a)], where the interdot distance $d = 288$ nm and $d = 312$ nm. The special locations for creating high concurrence generally satisfy $\Delta = -(2J + \Gamma/2)\tan(kd)$ and $kd = m\pi$ (m is an integer), which results in $|\xi_{k_1}| = |\xi_{k_2}|$. However, when n is 0.022, high concurrence can be maintained for any interdot distance d over several hundred nanometers. This is due to the fact that phase variation along the waveguide is very small for the plasmonic waveguide mode with a near-zero index. Moreover, in Fig. 5(b), the concurrence C for various Δ from $0.1J$ to $0.5J$ is shown when the mode index n is 0.022. Clearly, high concurrence C can be created for a wide range of the interdot distances d when Δ is $0.5J$. This means that a certain amount of QD waveguide

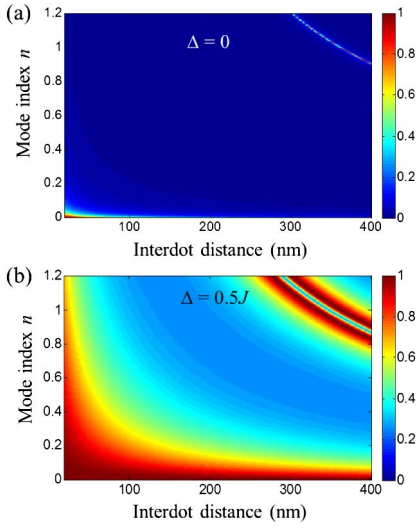

Fig. 3. Dependence of concurrence C on the plasmonic waveguide mode index n and the interdot distance d for (a) on-resonance case $\Delta = 0$ and (b) off-resonance case $\Delta = 0.5J$. Here $\Gamma = 0.01225J$ is used in the calculations.

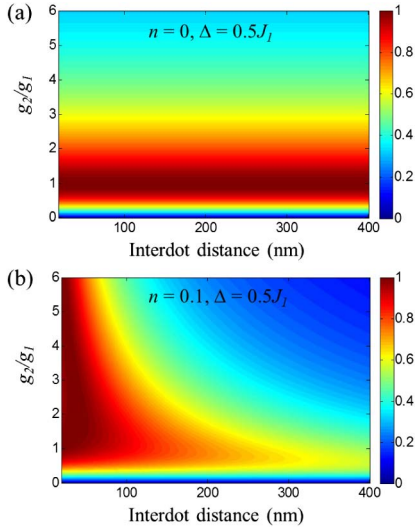

Fig. 4. Dependence of the concurrence C on the g_2/g_1 ratio and the interdot distance d when the plasmonic waveguide mode index (a) $n = 0$ and (b) $n = 0.1$. Here $\Gamma = 0.01225J_1$ is used in the calculations.

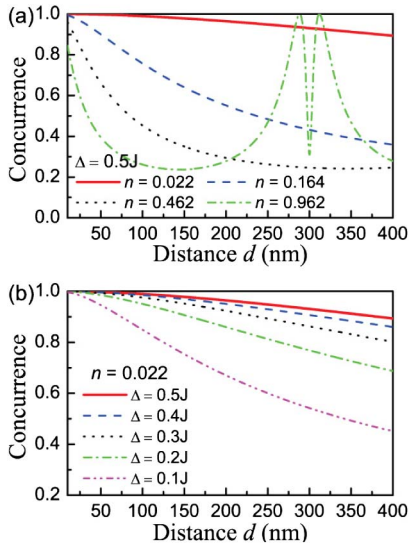

Fig. 5. (a) Dependence of the concurrence C on the interdot distance d when $\Delta = 0.5J$ for a different mode index n at 0.022 (red solid line), 0.164 (blue-dashed line), 0.462 (black-dotted line), and 0.962 (green dashed–dotted line); (b) dependence of the concurrence C on the interdot distance d when the mode index $n = 0.022$ for different QD waveguide detuning Δ at $0.5J$ (red solid line), $0.4J$ (blue-dashed line), $0.3J$ (black-dotted line), $0.2J$ (green dashed–dotted line), and $0.1J$ (magenta dashed–dotted–dotted line).

detuning in the experiment will not be detrimental to the high concurrence across large interdot distances as long as the QD–waveguide coupling strength is maintained.

In conclusion, we have examined quantum entanglement in SiO_2/Ag plasmonic waveguides with considerations of QD waveguide detunings, asymmetric coupling strengths, and dissipations. The waveguides can be designed to possess near-zero mode indices around the QD transitions, and high concurrence can be achieved between two QDs interacting with the plasmonic waveguide modes. A wide range of interdot distances are allowed for achieving high concurrence due to the near-zero phase variation along the waveguide, which shows advantages over the schemes implemented by dielectric waveguides or metal nanowires, where specific interdot distances are required. The plasmonic waveguide with near-zero mode indices serves as a great platform for solid-state quantum optics and quantum information processing.

This work was supported by Energy Research and Development Center at Missouri University of Science and Technology and the University of Missouri Research Board.

References

1. A. K. Ekert, Phys. Rev. Lett. **67**, 661 (1991).
2. C. H. Bennett, G. Brassard, C. Crépeau, R. Jozsa, A. Peres, and W. K. Wootters, Phys. Rev. Lett. **70**, 1895 (1993).
3. C. Nölleke, A. Neuzner, A. Reiserer, C. Hahn, G. Rempe, and S. Ritter, Phys. Rev. Lett. **110**, 140403 (2013).
4. E. Knill, R. Laflamme, and G. J. Milburn, Nature **409**, 46 (2001).
5. J. R. Petta, A. C. Johnson, J. M. Taylor, E. A. Laird, A. Yacoby, M. D. Lukin, C. M. Marcus, M. P. Hanson, and A. C. Gossard, Science **309**, 2180 (2005).
6. N. Akopian, N. H. Lindner, E. Poem, Y. Berlatzky, J. Avron, D. Gershoni, B. D. Gerardot, and P. M. Petroff, Phys. Rev. Lett. **96**, 130501 (2006).
7. E. Togan, Y. Chu, A. S. Trifonov, L. Jiang, J. Maze, L. Childress, M. V. G. Dutt, A. S. Sørensen, P. R. Hemmer, A. S. Zibrov, and M. D. Lukin, Nature **466**, 730 (2010).
8. H. Bernien, B. Hensen, W. Pfaff, G. Koolstra, M. S. Blok, L. Robledo, T. H. Taminiau, M. Markham, D. J. Twitchen, L. Childress, and R. Hanson, Nature **497**, 86 (2013).
9. H. Raether, *Surface Plasmons on Smooth and Rough Surfaces and on Gratings* (Springer, 1988).
10. S. I. Bozhevolnyi, V. S. Volkov, E. Devaux, J. Laluet, and T. W. Ebbesen, Nature **440**, 508 (2006).
11. D. E. Chang, A. S. Sørensen, P. R. Hemmer, and M. D. Lukin, Phys. Rev. Lett. **97**, 053002 (2006).
12. D. E. Chang, A. S. Sørensen, E. A. Demler, and M. D. Lukin, Nat. Phys. **3**, 807 (2007).
13. G. Y. Chen, C. M. Li, and Y. N. Chen, Opt. Lett. **37**, 1337 (2012).
14. X. R. Jin and J. Gao, Opt. Lett. **38**, 2110 (2013).
15. A. V. Akimov, A. Mukherjee, C. L. Yu, D. E. Chang, A. S. Zibrov, P. R. Hemmer, H. Park, and M. D. Lukin, Nature **450**, 402 (2007).
16. Y. Fedutik, V. V. Temnov, O. Schöps, U. Woggon, and M. V. Artemyev, Phys. Rev. Lett. **99**, 136802 (2007).
17. H. Wei, D. Ratchford, X. Li, H. Xu, and C. K. Shih, Nano Lett. **9**, 4168 (2009).
18. W. Chen, G. Y. Chen, and Y. N. Chen, Opt. Express **18**, 10360 (2010).
19. N. C. Kim, J. B. Li, Z. J. Yang, Z. H. Hao, and Q. Q. Wang, Appl. Phys. Lett. **97**, 061110 (2010).
20. G. Y. Chen and Y. N. Chen, Opt. Lett. **37**, 4023 (2012).
21. G. Y. Chen, N. Lambert, C. H. Chou, Y. N. Chen, and F. Nori, Phys. Rev. B **84**, 045310 (2011).
22. A. Gonzalez-Tudela, D. Martin-Cano, E. Moreno, L. Martin-Moreno, C. Tejedor, and F. J. Garcia-Vidal, Phys. Rev. Lett. **106**, 020501 (2011).
23. E. J. R. Vesseur, T. Coenen, H. Caglayan, N. Engheta, and A. Polman, Phys. Rev. Lett. **110**, 013902 (2013).
24. R. Horodecki, P. Horodecki, M. Horodecki, and K. Horodecki, Rev. Mod. Phys. **81**, 865 (2009).
25. W. K. Wootters, Phys. Rev. Lett. **80**, 2245 (1998).